Enhanced Displacement of Phase Separating Liquid Mixtures in 2D Confined Spaces

Gilmar F. Arends, Jae Bem You, John M. Shaw, and Xuehua Zhang*

Read Online

ACCESS | Metrics & More | Article Recommendations | Supporting Information

ABSTRACT: Displacing liquids in a confined space is important for technological processes ranging from porous membrane separation to CO_2 sequestration. The liquid to be displaced usually consists of multiple components with different solubilities in the displacing liquid. Phase separation and chemical composition gradients in the liquids can influence the displacement rate. In this work, we investigate the effects of liquid composition on the displacement process of ternary liquid mixtures in a quasi-2D microchannel where liquid−liquid phase separation occurs concurrently. We focused on model ternary mixtures containing 1-octanol (a model oil), ethanol (a good solvent), and water (a poor solvent). These

mixtures are displaced with water or with an ethanol aqueous solution. As a comparison, for some experiments, water was displaced by ternary mixtures. The bright-field and fluorescence imaging measurements reveal distinct phase separation behaviors. The spatial distribution of subphases arising from phase separation and the displacement rates of the solution are impacted by the initial ternary solution composition. The boundary between the solution and displacing liquid changes from a defined interface to a diffusive interface as the initial 1-octanol composition in the solution is reduced. The displacement rate also varies non-linearly with the initial 1-octanol composition. The slowest displacement rate arises at intermediate 1-octanol concentration, where a stable three-zone configuration forms at the boundary. At very low 1-octanol concentration, the displacement rate is fast, associated with droplet formation and motion driven by the chemical concentration gradients formed during phase separation. The excess energy provided from phase separation may contribute to the enhanced displacement at intermediate to high 1-octanol concentrations but not at low 1-octanol concentration with enhancement from induced flow in confinement. The knowledge gained from this study highlights the importance of manipulating phase separation to enhance mass transport in confinement for a wide range of separation processes.
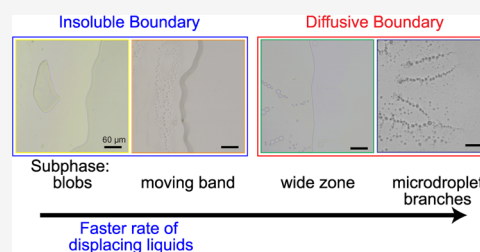
INTRODUCTION

Enhanced flow transport in confined spaces is important in many processes, from catalytic-based chemical conversion,[1] porous membrane separation,[2] nanomedicine,[3−5] and water treatment[6] to enhanced oil recovery[7,8] and CO_2 sequestration.[9,10] In confined spaces, liquid mixing is dominated by slow mutual diffusion,[11,12] influenced by the physical properties of liquids. Extensive studies have been performed to understand the effects of wettability of the wall surface,[6,12,13] fluid viscosity,[14,15] or interfacial tension of immiscible phases.[10] On an industrial scale, the liquid displaced from confined spaces usually consists of multiple chemical constituents that can interact with the displacing liquid.[15−17] For example, in enhanced oil recovery, chemical flooding processes use a displacing liquid to recover the entrapped oil phase from porous rocks by altering the interfacial tension or by reducing the viscosity of the pore fluid.[16,18] It is important for both fundamental understanding and practical applications to achieve fast fluid movement in confined spaces.

Enhanced fluid transport and autonomous motion of droplets and colloidal particles driven by chemical concentration gradients in multicomponent liquid mixtures[19] are topics of current research interest. Microparticles or microdroplets move as a result of diffusiophoretic or solutal-driven Marangoni phenomena.[19] Concentration gradients are often created and sustained by chemical reaction,[20] dissolution of surfactants,[21] and surface chemistry interactions.[22] Manipulating the electrolyte concentration in the displacing fluid has been demonstrated to drive colloid transport into and out of microchannel dead-ends.[23−25]

In addition to chemical concentration gradients present in multicomponent single-phase liquid mixtures, subphase formation from phase separation in multicomponent systems is also advantageous in displacing liquid in confined spaces. Even from a practical application perspective, several studies have indicated improvements in oil recovery efficiency from porous media when microdroplet emulsions are formed during displacement compared to cases without emulsion formation. In these cases, the enhancement effect is attributed to the desired rheological properties and seepage characteristics of

surfactant-stabilized emulsions.[17] More fundamentally, micro-droplets form spontaneously from the simple addition of a poor solvent into a ternary solution via the Ouzo effect. When the ternary solution is diluted by a poor solvent that is miscible with the solvent but immiscible with droplet liquid, the mixture becomes oversaturated, leading to the formation of many microsized droplets dispersed over the entire continuous liquid phase without the use of mechanical agitation or surfactant.[26−28] In confinement, the spontaneous formation of microdroplets leads to enhanced transport of the penetrating fluid.[27] While the effect has been demonstrated, it has not been explored in detail. It remains unclear how the displacement rate is influenced by the relative and absolute compositions of phases formed during phase separation—even for a single mixture.

In this work, we use a simple ternary liquid mixture as a model system to explore the displacement process in quasi-2D confined spaces. More specifically, the confined liquid comprises a ternary solution of 1-octanol, ethanol, and water. The displacing liquid is water. The displacement process is shown to be strongly dependent on the composition of the confined liquid. We demonstrate that over one range of compositions, the confined liquid is displaced. Over another range of compositions, we demonstrate the selective separation and displacement of 1-octanol. As the composition trajectories and hence the intersection points with the one-phase to the two-phase boundary in the phase diagram are known, our findings suggest that an effective approach to enhance mass transport in confined spaces is to use displacement liquid composition as a design variable.

■ EXPERIMENTAL SECTION

Chemicals and Solution Preparation. Chemicals were used as received without further purification. Solution A consisted of 1-octanol (ACS grade > 95%, Fisher Scientific), ethanol (Histological grade, Fisher Scientific), and (Milli-Q) water. The compositions of solution A were varied from 2% 1-octanol to 50% 1-octanol as listed in Table 1. Solution B consisted of (Milli-Q) water. Additional experiments were performed with variations to both confined and displacing liquids, as summarized in Table 2.

Table 1. Evaluated Experimental Compositions of Solution A (Displaced Liquid) by Mass Percentage

composition	1-octanol, mass %	ethanol, mass %	water, mass %
1	50	40	10
2	40	45	15
3	35	48	17
4	30	48	22
5	25	48	27
6	20	48	32
7	15	48	37
8	10	48	42
9	8	47	45
10	5	48	47
11	2	48	50

The surfaces used for the experiments were hydrophilic glass slides (Fisherbrand Microscope Slides) and hydrophobic silicon wafers. Before use, both substrates were initially washed with piranha solution consisting of 70% vol H_2SO_4 (ACS Plus grade, Fisher Scientific) and 30% vol H_2O_2 (30% ACS grade, Fisher Scientific) at 85 °C for 20 min (caution: piranha solution is highly caustic). They were further cleaned and sonicated with water and ethanol each for 15 min. To

Table 2. Compositions of Solution A (Displaced Liquid) and Solution B (Confined Liquid) by Mass Percentage in Additional Experiments

composition	solution A			solution B		
	1-octanol	ethanol	water	1-octanol	ethanol	water
E1	50	40	10	0	25	75
E4	10	48	42	0	25	75
R1	0	0	100	50	40	10
R4	0	0	100	10	48	42

render the silicon wafers hydrophobic, they were coated with octadecyltrichlorosilane (OTS-Si), as has been previously documented.[29] In brief, 0.5% vol of OTS in hexane mixture was used to soak the wafers for 12 h at room temperature. The OTS-Si substrates were then sonicated with hexane, acetone, and ethanol for 10 min each to remove any excessive OTS on the surface.

For fluorescence experiments, Nile red (Fisher Scientific) was used due to its high solubility in hydrocarbon-rich phases where the oil-rich domains become fluorescent, which is useful for identifying liquid regions rich in 1-octanol.

Dimensions and Setup of the Microchamber. The flow chamber, as sketched in Figure 1, consisted of a polycarbonate base
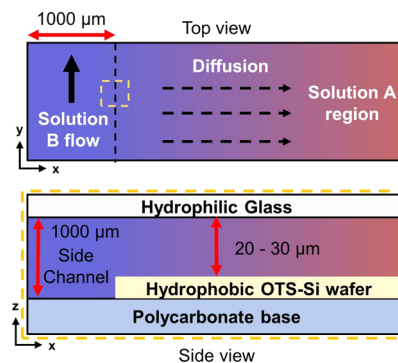

Figure 1. Sketch of the fluid microchamber with top view and cross-section of the main and side channels.

(8.5 × 4.5 × 1 cm) with the hydrophilic cover glass as the top sealed with a silicon rubber spacer. Before any experimentation, every component from the chamber was sonicated in both water and ethanol for 10 min each. The chamber was assembled by connecting the tubing to the polycarbonate base as the inlet and outlet streams. A droplet of solution A was placed on the OTS-Si substrate. The substrate was held by a capillary bridge to the cover glass. A small channel height of around 20−30 μm was kept. The cover glass was then held in position by a spacer and was clamped to the base of the chamber with large binder clips.

Process of the Liquid Displacement. Solution B was pumped using a syringe pump (Fisherbrand Single Syringe Pump) to the channel. The displacement process as water diffused transversely into the narrow channel was captured in situ using a camera (Nikon DS-Fi3) connected to an optical microscope (Nikon Eclipse Ni-U). The magnification under normal conditions was 10× with a F.O.V. of 22 mm, and videos were captured using an auto-exposure setting leading to captured footage with frame rates ranging from 10 to 15 frames per second (fps) at a fixed resolution of 2880 × 2048. Fluorescence footage required longer exposure times to capture the fluorescent features leading to low frame rates of 0.9−1 fps.

Analysis of the Displacement Rates. The videos were processed through ImageJ by converting them to image sequences. If required, the contrast and brightness levels were adjusted, and a bleach correction was applied. The tracking of the boundaries was achieved by the manual tracking plugin within the program. The calibration used for the captured footage at 10× magnification was
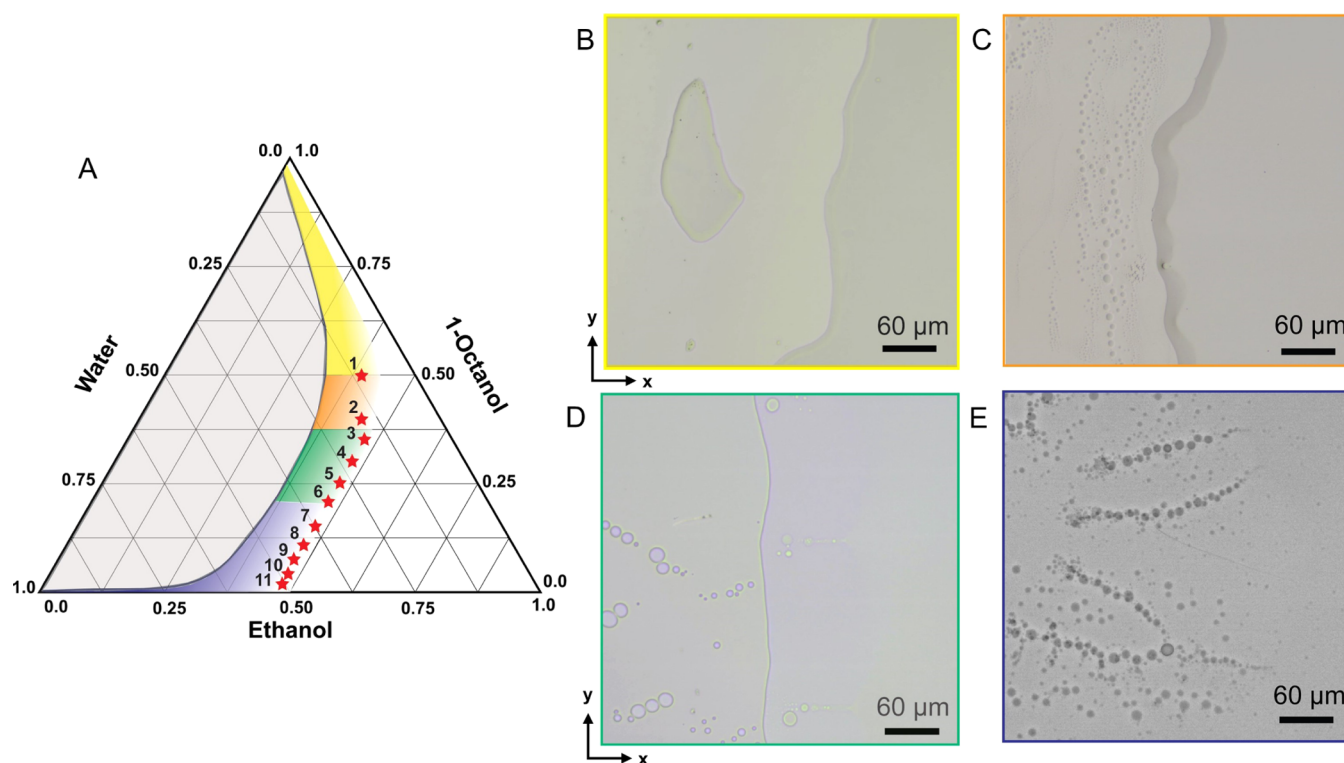
Figure 2. Overview of different dynamic regimes. (A) Ternary phase diagram of 1-octanol, ethanol, and water systems in terms of mass fractions with evaluated experimental compositions annotated. Displacement regimes are indicated by colors: regime 1 (yellow), regime 2 (orange), regime 3 (green), and regime 4 (blue). Reproduced from *ACS Cent. Sci.* **2016**, *2*, 7, 467−475 (ref 30). Copyright 2016 American Chemical Society. (B−E) Representative optical images of the phase separation regimes are shown in color-coded rectangles as in (A).

0.24 px/μm. The tracked data were saved as a raw CSV file, including the number of frames and x and y positions in pixels. The displacement rate was calculated using the x and y positions using the first entry in the data set as the initial position.

■ RESULTS AND DISCUSSION

The phase diagram for the model ternary mixture 1-octanol (oil), ethanol (good solvent), and water (poor solvent) is illustrated in Figure 2A. Confined liquid compositions labeled from 1 to 11 (Table 1) are shown in the phase diagram. The phase boundary was adapted from the literature,[30] tie lines not shown were computed using the UNIFAC model and inform the discussion. The Dortmund UNIFAC model was implemented using the parameter values noted in the Supporting Information (Tables S1−S4).

The mixing between solution A and water as water diffused into the narrow channel induced liquid−liquid phase separation. In the following sections, we show the displacement process along with phase separation for the wide range of solution A compositions listed in Table 1. The 1-octanol-rich liquid is revealed using a hydrophobic dye in fluorescence images. The displacement dynamics are categorized into four regimes, as shown in Figure 2B−E.

Regime 1: Receding Interface. Regime 1 corresponds to a high 1-octanol concentration, above 50% by mass in solution A. The composition is labeled in the phase diagram in Figure 3A. As water diffused from the side channel, the resulting images in Figure 3B show a clear interface separating solution A from water in the narrow channel.

A few 1-octanol microdomains pinched off from the receding phase boundary at several locations and remained attached to the hydrophobic wall on the water side of the

boundary. Their composition was confirmed using fluorescence imaging (Figure 3C). This fluorescence image of a representative domain formed from solution A doped with an oil-soluble fluorescent dye (Nile red). The high fluorescence intensity from the microdomain indicates the high concentration of the dye in the microdomain, in contrast to the absence of a fluorescence signal from the surrounding liquid. The spatial distribution of the dye is consistent with the chemical composition of the 1-octanol-rich microdomains surrounded by water-rich liquid.

In this regime, water diffusing into the narrow channel did not lead to liquid−liquid phase separation along the boundary—a behavior consistent with that of an immiscible displacing liquid. However, liquid−liquid phase separation did occur within the stranded microdomains. Many nanodroplets (with a diameter of approximately 4 μm) formed, as shown in Figure 3D. The formation of these water-rich nanodroplets is attributed to subphase formation arising from the diffusion of water into the microdomains followed by liquid−liquid phase separation.

As water diffuses into a microdomain and 1-octanol and ethanol diffuse out, the global composition of the microdomain changes. To a first approximation, the dilution path that is followed is indicated by the dashed line in the phase diagram in Figure 3A. The mixture becomes unstable as the composition intersects the solubility curve and spontaneously forms water-rich and 1-octanol-rich subphases. Although the global composition of the microdomain at separation is unknown, the compositions of the 1-octanol-rich and water-rich subphases created are approximately 80 and 19% 1-octanol by mass. It is interesting that phase separation occurred in the microdomains of stranded solution A but not at the boundary
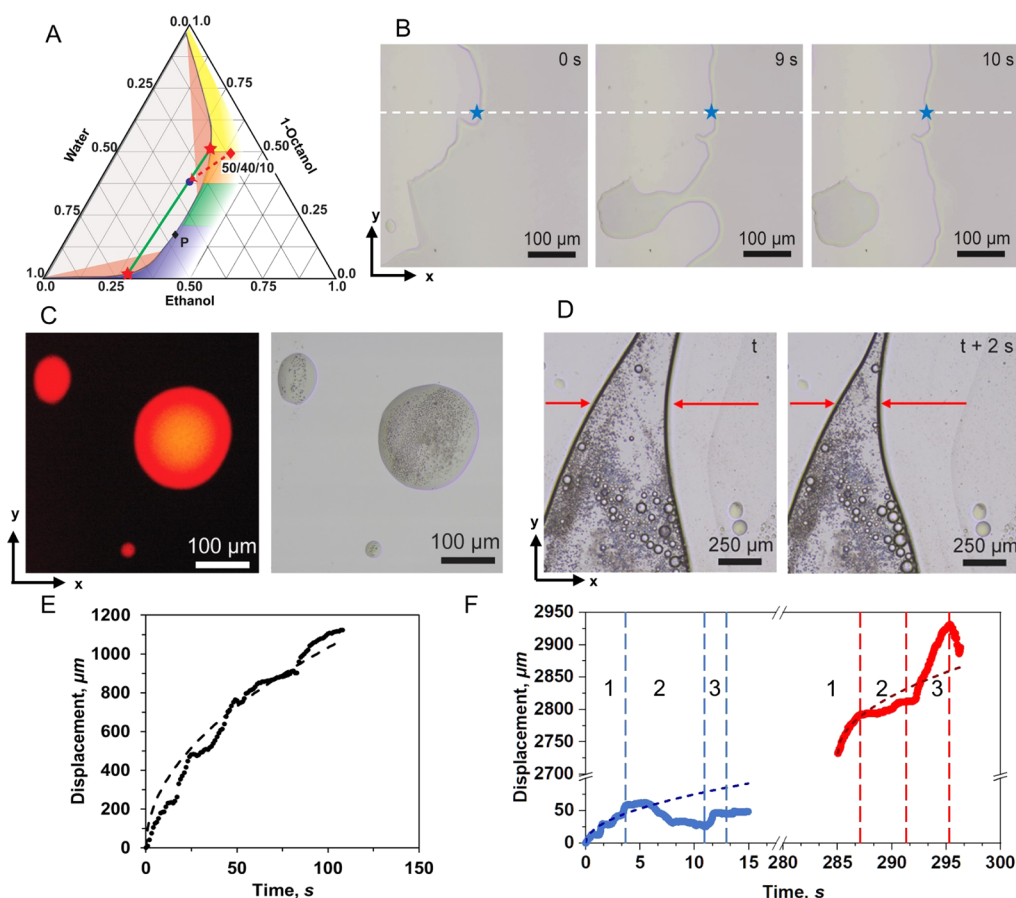
Figure 3. Overview of regime 1. (A) Ternary phase diagram indicating the dilution path with the two macroscopic subphases formed. *P* is the plait point of the ternary mixture. Red regions within the phase envelope are the Ouzo and reverse Ouzo regions. The initial solution A composition is given by a red diamond. An illustrative unstable mixture composition during dilution is given as a blue diamond. The red stars represent the 1-octanol-rich and water-rich compositions formed along the green tie line. Reproduced from *ACS Cent. Sci.* **2016**, *2*, 7, 467−475 (ref 30). Copyright 2016 American Chemical Society. (B) Time-based optical images of early film and domain development. (C) Side by side fluorescence and bright-field images of representative microdomains. (D) Time-based images of a deformed domain narrowing with time. (E) Plot showing local boundary displacement without microdomain formation. (F) Plot showing local boundary displacement at a location where microdomains form. Blue data set was taken along the *x*-direction indicated by a white dashed line in (B) with the same reference position of the side channel. Time window 1 is for a period without a microdomain present. During time period 2, a microdomain forms at the boundary. Time period 3 starts as soon as the microdomain detaches from the boundary. The formation of microdomains slows boundary displacement. Their detachment accelerates boundary displacement.

between water and solution A. The large surface to volume ratio of the small microdomains permits them to become supersaturated with water quickly. By contrast, at the boundary, water diffuses into the bulk 1-octanol-rich phase, and 1-octanol and ethanol diffuse into the bulk water-rich phase. Consequently, the liquids on both sides of the boundary do not supersaturate within the time frame of measurements. At longer times, one would certainly expect the microdomains to dissolve into the water-rich phase.

While the shape and size of stranded solution A microdomains varied between experiments (Figure 3D) possibly due to the nature of the interface instability—subphase formation within them over time was common.

If we now focus on the displacement of the boundary between solution A and water, in the absence of microdomain formation, we can see that the *x*-location displacement rate is essentially time-invariant with an average value of 10.7 ± 0.3 μm/s (Figure 3E). Figure 3F shows the fluctuating *x*-location displacement rate where microdomains form and detach over time. The interface progressively displaced solution A in the positive *x*-direction. During the formation of a microdomain,

the interface remains stationary or moves backward. When a microdomain detaches from the interface, the interface accelerates in the positive *x*-direction. Such cycles were observed at multiple locations on the surface.

The blue and red dashed curves in Figure 3F are 1D diffusion-based displacement curves, $l = (2Dt)^{1/2}$, fitted to the interface displacement data before microdomain detachment to obtain an effective diffusion constant.[27] The effective diffusivity varies as the boundary progresses. The values range from 5.3×10^{-9} m^2/s for a part of the boundary without microdomain formation (Figure 3E) and 2.8×10^{-10} to 7.9×10^{-10} m^2/s for a location where there is microdomain formation. The mutual diffusivities of water and ethanol and water and octanol range from 1.08×10^{-10} to 1.23×10^{-9} m^2/s and 2.0×10^{-10} to 7.3×10^{-10} m^2/s, respectively.[31−33] So, the diffusion rates are consistent with expectations. In locations with microdomain formation, the boundary displacement rate was variable and ranged from 4.3 to 14.0 μm/s.

The influence of solution A microdomains on the local motion of the boundary may be attributed to the pinning effect and mass transfer to microdomains. Imperfections on the wall
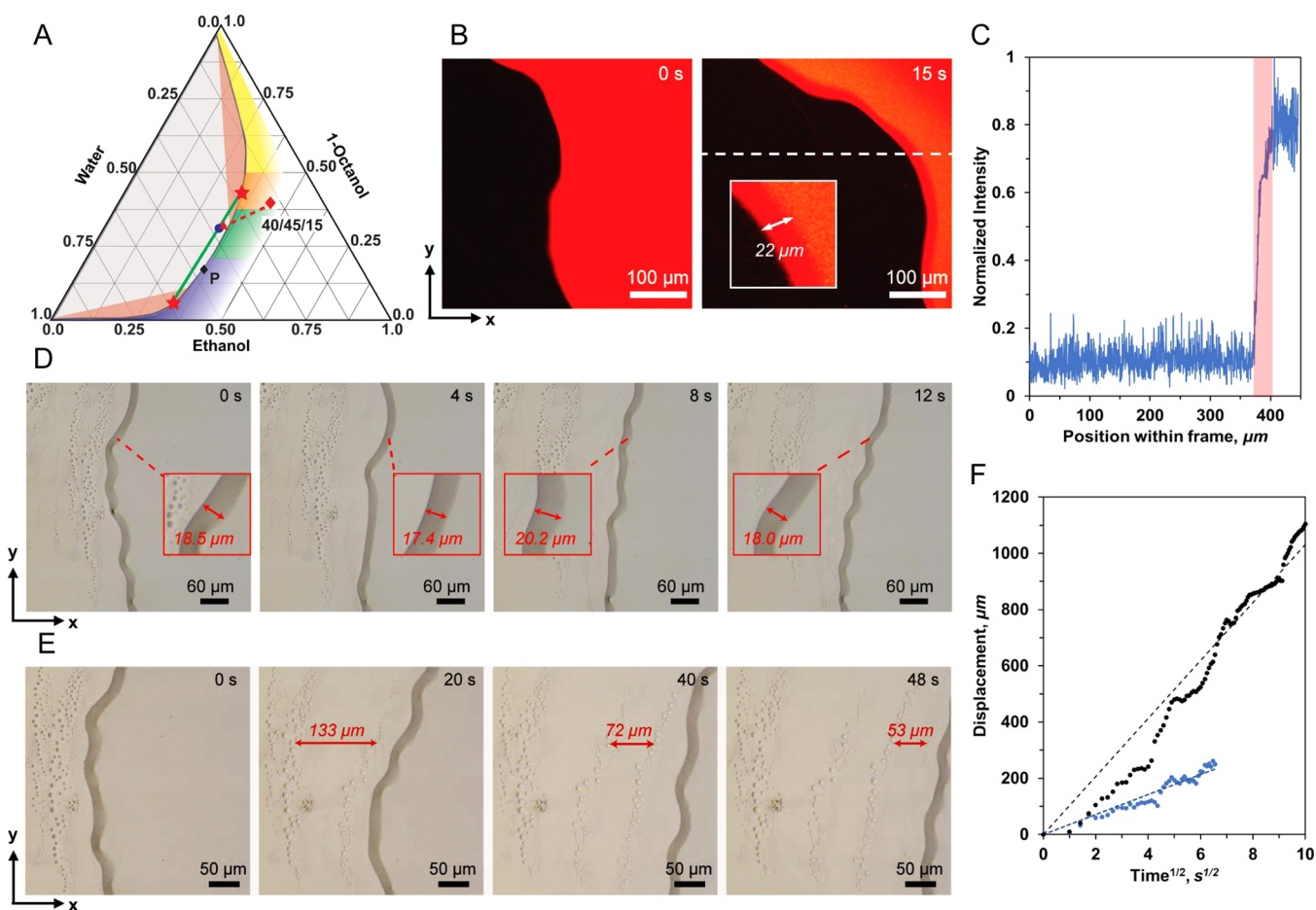
Figure 4. Overview of regime 2. (A) Ternary phase diagram indicating the approximate dilution path and the compositions of the subphases formed. *P* is the plait point of the ternary mixture. Red regions within the phase envelope are the Ouzo and reverse Ouzo regions. The initial solution composition is given by a red diamond. The unstable mixture composition after dilution is approximated by a blue diamond. The red stars represent the 1-octanol-rich and water-rich subphases that are formed based on the green tie line. Reproduced from *ACS Cent. Sci.* **2016**, *2*, 7, 467−475 (ref 30). Copyright 2016 American Chemical Society. (B) Time-based fluorescence imagery at 40% 1-octanol within regime 2. (C) Normalized fluorescence intensity as a function of *x*-location within the frame of (B) at *t* = 15 s. The red area in the graph indicates a boundary zone. (D) Time-based optical images of moving boundary within regime 2 with an initial solution A composition of 40% 1-octanol. The inset contains magnified images of the moving boundary indicating zone thickness. (E) Time-based optical images of droplet formation in the boundary zone. (F) Boundary displacement as a function of the square root of time assuming diffusion-based dynamics. (Black) indicates Regime 1 smooth interface displacement and (Blue) Regime 2 boundary displacement.

surface pin the boundary, leading to microdomain formation once the boundary becomes unstable. As the microdomain is formed, the water-rich phase close to the microdomain experiences interfacial tension opposite to its flow direction. The acceleration experienced after the detachment of the microdomain may be attributed to the release of built-up tension that comes from the stretched interface of the microdomain.

In regime 1, water largely displaces solution A (with a high initial concentration of 1-octanol) in a confined space with one hydrophobic wall. The large-scale stability of the boundary between solution A and water contributes to the effective displacement. In contrast, local instability of the boundary and microdomain formation leads to lower and fluctuating displacement rates indicated in Figure 3F, as well as less efficient 1-octanol-rich liquid displacement.

Regime 2: Moving Microdroplet Zone. Regime 2 corresponds to intermediate 1-octanol concentrations, about 40% by mass in solution A. The overall behavior in regime 2 differs markedly from regime 1, despite the similarity of

solution A compositions. Starting from this composition, the subphase formed by mixing with water is well approximated by the trajectory shown in Figure 4A. From the tie line shown in the phase diagram, much more 1-octanol-rich subphase is still expected than water-rich subphase following liquid−liquid phase separation. Unlike regime 1, a mobile 1-octanol-rich microdroplet zone separates solution A and water throughout the narrow channel, as shown in the fluorescence images in Figure 4B. A dark zone containing water, a zone rich in microdroplets, and a clear zone of solution A are clearly present.

Figure 4C shows the level of fluorescence intensity crossing the three zones. The high fluorescence intensity in the intermediate zone confirms that it is rich in 1-octanol. The boundary zone appears dark in bright-field images possibly due to scattering from small 1-octanol-rich drops.

The time-based images in Figure 4D show oscillation of the boundary zone, but this oscillation does not lead to the formation of stranded microdomains. Instead, the boundary zone thickness appears to remain constant at 18−20 μm in the
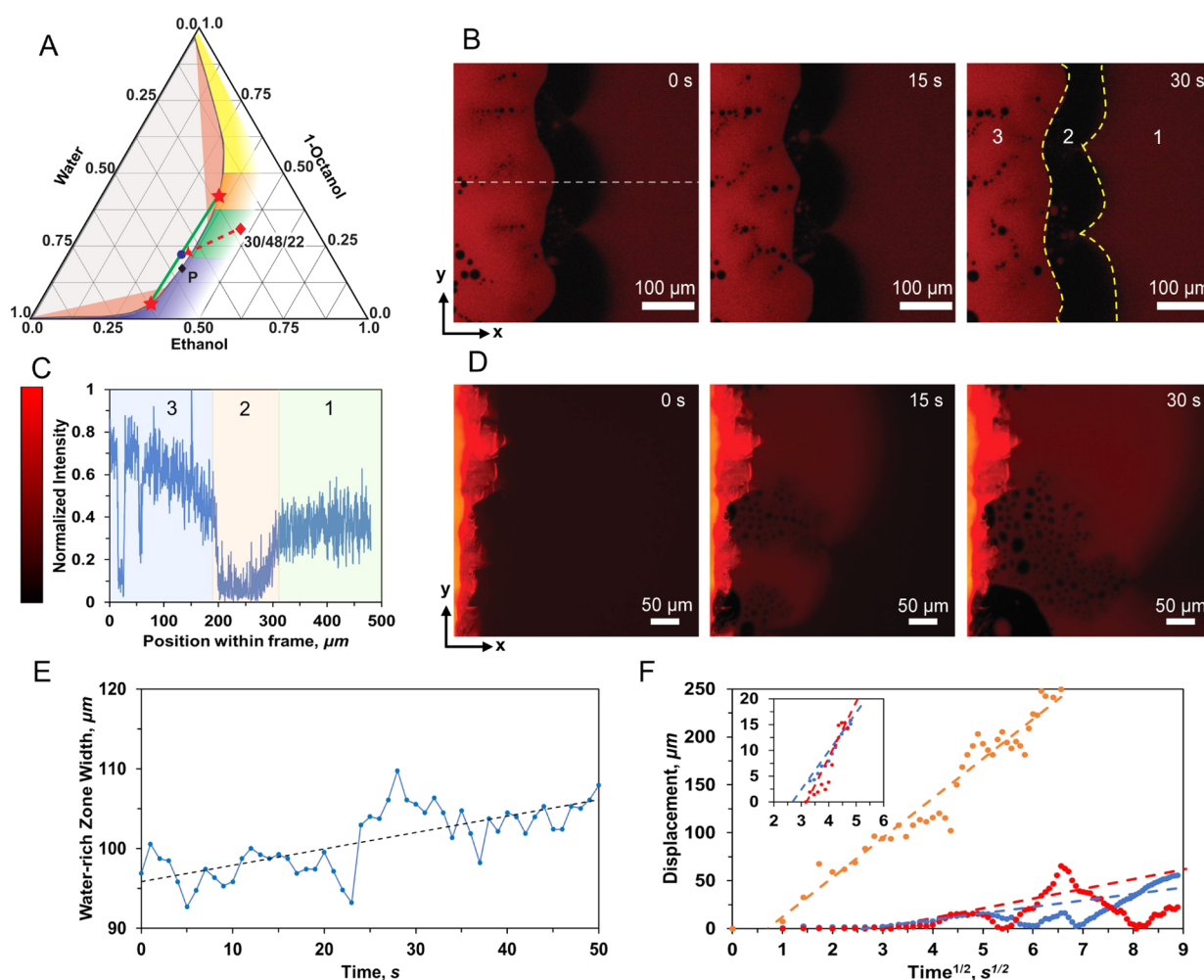
Figure 5. Overview of regime 3 and dynamic data for 30% 1-octanol in solution A. (A) Ternary phase diagram showing the approximate dilution path and subphase compositions. *P* is the plait point of the ternary mixture. Reproduced from *ACS Cent. Sci.* **2016**, *2*, 7, 467−475 (ref 30). Copyright 2016 American Chemical Society. (B) Illustrative time-based fluorescence images for regime 3. Zone 1 is a 1-octanol-rich phase, zone 2 is a water-rich phase, and zone 3 is 1-octanol-rich liquid with dispersed water-rich phase drops. (C) Normalized fluorescence intensity as a function of *x*-location within the frame of (B) at *t* = 0 s. (D) Time-based fluorescence images showing stages as water begins to enter the narrow channel. (E) Water-rich zone 2 width as a function of time (dashed line indicating slight increasing trend). (F) Boundary displacement as a function of the square root of time illustrating diffusion-dominated movement. (Blue) corresponds to the boundary between zones 1 and 2. (Red) corresponds to the boundary between zones 2 and 3. (Orange) corresponds to regime 2 displacement data. Inset depicts the slopes, from $2 < t^{1/2} < 6$ for the boundaries in regime 3.

time interval of 12 s as the boundary moves forward, as shown in the high-magnification inset (Figure 4D). The time invariance of the boundary zone thickness may indicate that the mass transfer occurring through the boundary is balanced, even though the compositions of the water-rich and 1-octanol-rich phases in the zone vary along the *x*-direction.

Lines of stranded 1-octanol-rich droplets form behind the receding boundary zone, mirroring the shape of the boundary as it progresses (Figure 4E). The interval between two lines of droplets on the surface may be related to the time required for phase separation to occur in the boundary zone or the time required for the droplets inside the boundary zone to accumulate on the contact line with water.

The rate of the boundary displacement is quantified in Figure 4F along a fixed line in the *x*-direction. The rate of displacement fluctuates with time due to the oscillatory advancement of the boundary zone. Again, the data can be fitted with a diffusion model.[27] Compared to the displacement of the boundary in regime 1 (for a case where microdomain formation does not occur), the displacement versus square root of time is slower in regime 2. This is evidenced by the lower effective diffusivity obtained from the fit, which ranged from 5.8×10^{-10} to 6.7×10^{-10} m^2/s, and a lower displacement rate of 5.8 μm/s.

Regime 3: Moving Three-Zone Configuration. Regime 3 arises for the 1-octanol concentration range 20−30% by mass in solution A. Data for the 30% case are presented in detail and are representative of this regime. Figure 5A illustrates the dilution process within the phase diagram. On separation, approximately equal amounts of water-rich and 1-octanol-rich subphases form because the dilution line intersects the phase envelope close to the plait point.

Fluorescence images in Figure 5B reveal three distinct zones along the *x*-direction as labeled in Figure 5B at *t* = 30 s. The normalized fluorescence intensity plotted in Figure 5C shows that zone 1 consists of a 1-octanol-rich phase revealed by partition of the dye,[34] zone 2 consists of a water-rich subphase, and zone 3 contains numerous immiscible water-rich droplets
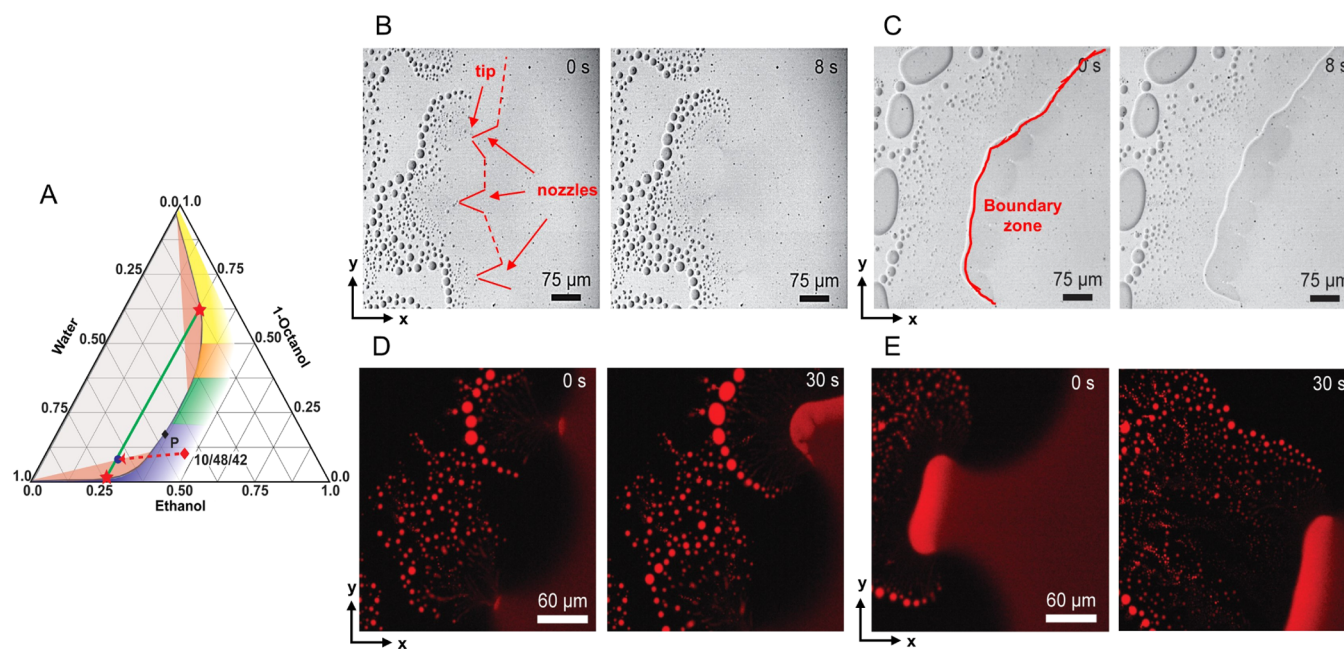
Figure 6. Overview of regime 4 at low 1-octanol compositions. (A) Ternary phase diagram indicating the approximate dilution path and subphase compositions. *P* is the plait point of the ternary mixture. Reproduced from *ACS Cent. Sci.* **2016**, *2*, 7, 467−475 (ref 30). Copyright 2016 American Chemical Society. (B) Time-based optical images showing boundary development and (C) boundary for the 10% 1-octanol solution A case. (D) Time-based fluorescence imagery of protrusion and change to (E) line-shaped boundary for the 10% 1-octanol case.

(dark features in fluorescence images within a 1-octanol-rich phase).

Figure 5D illustrates the early development of the three-zone configuration as water enters from the side to the narrow channel. A 1-octanol-rich phase forms from phase separation and water droplets appear simultaneously within the 1-octanol-rich subphase and later coalesce and merge into a water-rich zone 2.

The displacement of solution A proceeds as the entire zone 2 moves into the narrow channel. The width of zone 2 appears to increase slightly with time at a fixed *y*-position, as shown in Figure 5E. The most noticeable aspect of the entire zone 2 is its stability in space over minute-long time scales. We suspect that this stability is related to the near-constant width of zone 2, which we in turn attribute to the near equivalence of the influx and outflux of liquid to zone 2 over time. Liquid may enter zone 2 in the form of water-rich droplets from zone 3 or by water entering from the side channel, as evidenced in Figure S2. Concurrently, the 1-octanol-rich liquid leaves zone 2 to zone 3. The balancing of mass fluxes in and out of zone 2 accounts for its stability.

The displacement of zone 1 to zone 2 and zone 2 to zone 3 boundaries versus the square root of time are shown in Figure 5F. These boundaries move with an oscillatory behavior in the positive *x*-direction with a slower overall rate than the previous regime 2 at 0.71 μm/s. The fluctuations were found to be related to the water-rich droplets entering zone 2. At locations where droplets merged with the boundary between zone 2 and 3, the boundary retracted in the negative *x*-direction. The boundary successively becomes deformed, leading to the acceleration of the boundary in the positive *x*-direction as the shape of the boundary starts to recover. The boundary displacement curves from the two locations in Figure 5F show similar trends in pinning and depinning transitions. Regardless of all fluctuations in boundary motion, the three-zone

configuration remained stable with time due to water replenishment.

Regime 4: Diffusive Boundary. In regime 4, the composition ranges from 2 to 20% 1-octanol by mass in solution A. In this regime, a diffusive boundary forms and the dynamics differ from the other three regimes. The results depicted in Figure 6 are for 1-octanol for 10% by mass.

Figure 6A shows the approximate dilution path and subphase compositions in the phase diagram for the 10% 1-octanol case. The diluting mixture intersects the phase envelope below the plait point, and following phase separation, the water-rich subphase fraction is expected to be an order of magnitude greater than the 1-octanol-rich subphase mass fraction.

Figure 6B shows the diffusive boundary at an early transition stage consisting of numerous triangular protrusions of solution A that extend into the water phase. Droplets formed from the tips of these protrusions in the water-rich phase were larger than those formed at other positions along the boundary because, at the tip of the protrusions, the concentration gradients are sharper than at other positions.[26,27] At longer times, protrusions approach one another and collapse into a line-shaped boundary region, as shown in Figure 6C. At longer times, droplets are formed along the entire boundary in the water-rich phase.

Fluorescence images in Figure 6D,E show the 1-octanol-rich protrusions with a 1-octanol concentration greater than in solution A. Ethanol transfers preferentially to the water-rich phase. After 30 s, the composition of the protrusions becomes consistent with that of the 1-octanol rich droplets formed, as indicated by fluorescence intensity.

Figure 7A provides an overview and dynamic data for solution A with 2% 1-octanol. Figure 7A shows the approximate dilution path and subphase compositions. The mass ratio of water-rich to 1-octanol-rich subphase is expected to be around 25:1 in this case. Fluorescence images in Figure
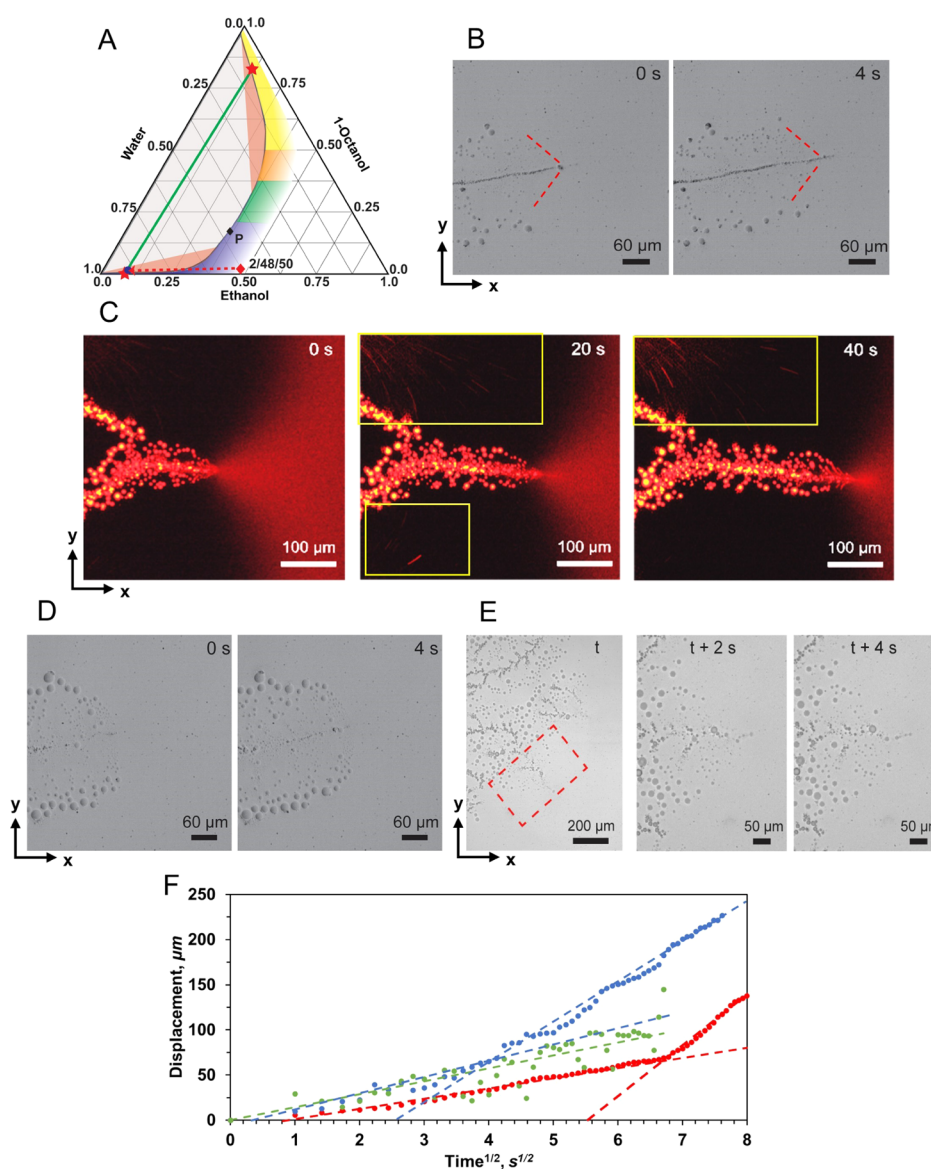
Figure 7. Regime 4 dynamics with a focus on low 1-octanol wt %. (A) Ternary phase diagram indicating the approximate dilution path and subphase compositions for solution A with an initial 1-octanol composition of 2% by mass. Reproduced from *ACS Cent. Sci.* **2016**, *2*, 7, 467−475 (ref 30). Copyright 2016 American Chemical Society. (B) Time-based optical images of triangular-shaped boundary movement using 2% by mass in solution A. (C) Time-based fluorescence images of 2% 1-octanol by mass indicating the 1-octanol-rich and water-rich regions. Yellow boxes show droplets recirculating back to the boundary region. Time-based optical images comparing the (D) 5% 1-octanol and (E) 8% 1-octanol conditions. (F) Boundary displacement as a function of the square root of time plot comparing the 2% octanol (blue), 5% (green), and 10% (red) conditions. Dashed lines show anticipated two-tiered diffusion-based displacement dynamics.

7C again show triangular protrusions of 1-octanol-rich liquid into the boundary. While the outcomes are similar to those described in Figure 6, the triangular protrusions are more stable (Figure 7B). This outcome is consistent with earlier work showing that droplets form branches from a diffusion-limited nucleation and growth process in a 2D confinement at low concentration.[35]

Once formed, numerous droplets traveled toward the side channels in the negative *x*-direction before becoming immobilized on the wall surface or coalescing with other droplets. The lines with low fluorescent intensity indicated in the yellow boxes in Figure 7C show induced droplet flow. The droplets appear as lines due to the exposure time of the camera when taking fluorescence imagery. This induced flow may

explain the relatively fast boundary displacement rate associated with regime 4.

The optical images in Figure 7D,E indicate the qualitative similarity of droplet formation and boundary movement phenomena for 5 and 8% 1-octanol by mass in solution A. Differences arise from the number of droplets formed and droplet size with time.

The displacement of the boundary is plotted against the square root of time for the 2, 5, and 10% initial 1-octanol wt % cases. As indicated by the slopes added to each curve in Figure 7F, a slower followed by a more rapid diffusive displacement process is clearly evident for the 2 and 10% conditions. While qualitatively similar, the first diffusion-controlled process slows and has a longer duration as the initial 1-octanol wt % increases. In regime 4, boundary displacement is faster than
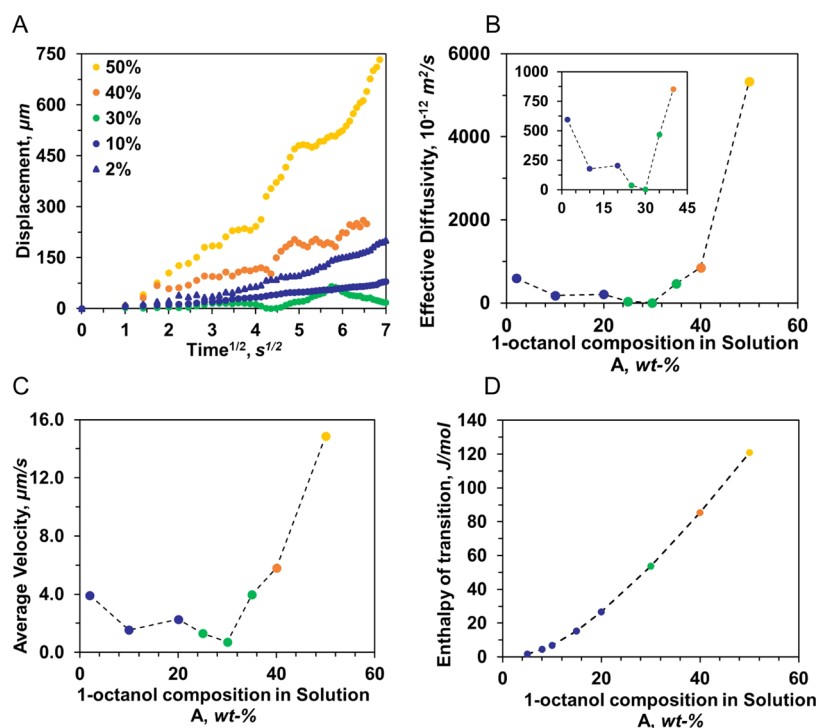
Figure 8. (A) Summary of displacement vs square root of time for 1-octanol compositions spanning the four regimes. (B) Effective diffusivity and (C) average velocity calculated from displacement vs time data in all four regimes. (D) Calculated enthalpy of transition from a nonequilibrium single-phase state to two-equilibrium states based on the Dortmund UNIFAC method.

regime 3 compositions, and there are seldom oscillations in displacement versus time plots.

Comparison of the Displacement Rates in the Four Regimes. In Figure 8A, we compare the displacement rates in all four regimes presented. An effective diffusivity was calculated for each regime, as shown in Figure 8B. The highest effective diffusivity value was obtained in regime 1 at 50% of 1-octanol for a smooth boundary, which has an enhanced effective diffusivity of 8×10^{-9} m^2/s. The effective diffusivity obtained is thus higher than the expected range of the mutual diffusivities between water and ethanol (1.1×10^{-10} to 1.2×10^{-9} m^2/s) and water and 1-octanol (2.0×10^{-10} to 7.3×10^{-10} m^2/s) showing enhanced diffusion. In both high and low 1-octanol ratios of regimes 1 and 4, the displacement rate of the boundary was faster at ~15 and ~4 μm/s. In contrast, in the intermediate regime 3, the rate is only ~0.7 μm/s as shown by the average velocities in Figure 8C. Boundary displacement in regime 3 is slower than in the other regimes but remains 2 times the displacement rate expected for a purely diffusive single-phase process obtained from the effective diffusivity.

To understand the dependence of displacement rate on 1-octanol concentration, including a shallow minimum at intermediate 1-octanol concentrations, we must consider competing effects. Differences in the energy released during phase separation with 1-octanol concentration are illustrated in Figure 8D. The energy released during the transition from a nonequilibrium single-phase state to an equilibrium two-phase state increases with 1-octanol concentration. To the extent that displacement rate depends on this thermodynamic driving force, one would anticipate an increase in displacement rate with 1-octanol concentration. This effect is clearly evident at high 1-octanol concentration. However, the displacement rate at low 1-octanol concentrations is somewhat higher than at

intermediate 1-octanol concentrations. We attribute this apparent enhancement in displacement at low 1-octanol concentrations to droplet propulsion and the flow induced in the continuous phase from the self-propelling microdroplets in this concentration range, that is, to how the energy of phase transition is dissipated.

Impacts of relative viscosity of the liquid phases and the relative wettability of the liquid phases on the wall surface, which approach one at intermediate 1-octanol concentrations (near the plait point), are seen as secondary. Viewed from this perspective, the strong dependence of displacement rate on the initial composition is expected to be a general feature for displacing multicomponent liquids undergoing phase separation. Furthermore, compositions transitioning through regimes 1 and 2 are preferred for displacing liquid, while compositions transitioning through regimes 3 and 4 are preferred for promoting the separation and extraction of a component or a component category (1-octanol, a model oil in this case) from the solution at lower overall displacement rates.

We note that the 1-octanol/ethanol/water chemical system is complex, and there has been extensive study on how chemical composition affects the molecular-level structures of single-phase solutions near the phase envelope.[28,30,36−38] Compared to the work by Lopian et al., in our regime 1, the initial compositions correspond to a reverse aggregate regime in their work. Regime 2 compositions would be those transitioning from the reverse aggregate to the bicontinuous regime. Regime 3 would be within the bicontinuous regime, and regime 4 would be considered the pre-Ouzo compositions. However, we were not able to directly link the displacement rate to the structures of microemulsions in space and in time. The reason is that the structures of microemulsions are on a molecular-level scale, whereas our experimental observations
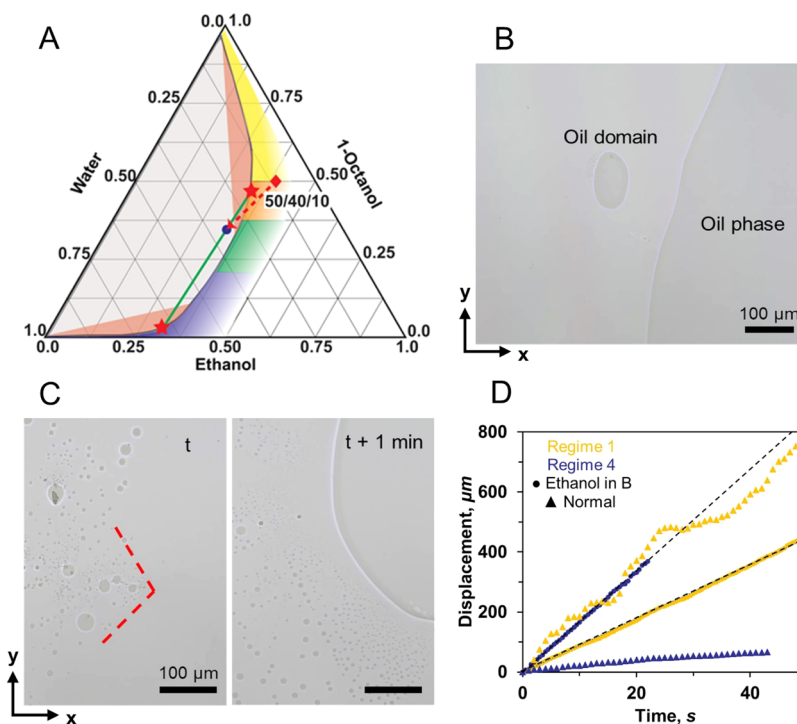
Figure 9. (A) Ternary phase diagram indicating the approximate dilution path using 25% ethanol in the displacing liquid at regime 1 condition. Reproduced from *ACS Cent. Sci.* **2016**, *2*, 7, 467−475 (ref 30). Copyright 2016 American Chemical Society. (B) Optical image of regime 1 condition using 25% ethanol by mass in the displacing liquid. (C) Time-based optical images of regime 4 conditions using 25% ethanol by mass in the displacing liquid. (D) Boundary displacement as a function time for ethanol in displacing liquid comparing the 10% 1-octanol (blue) and 50% (yellow) conditions. Dashed lines indicate linear regression from data. Data for pure water as displacing liquid in both regimes was added for comparison (triangles).
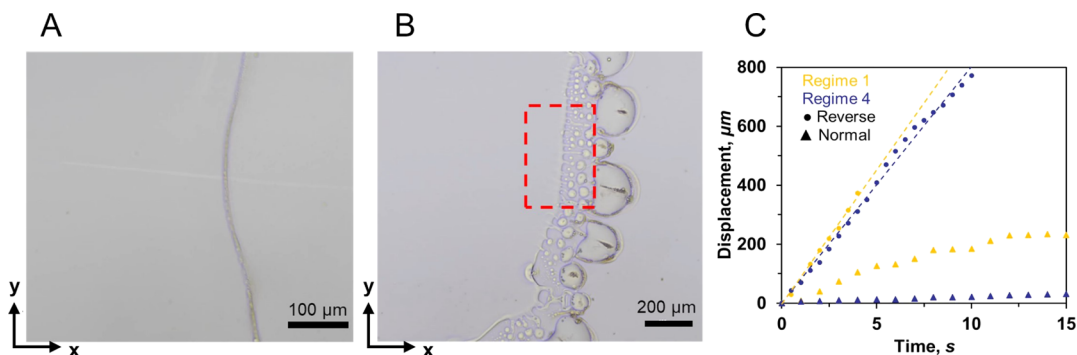

Figure 10. (A) Optical image showing confined water being displaced by solution A with a 50% 1-octanol by weight composition. (B) Optical image showing confined water being displaced by solution A with a 10% 1-octanol by weight composition. (C) Boundary displacement as a function time for reverse conditions comparing the 10% octanol (blue) and 50% (yellow) conditions. Dashed lines indicate linear regression of data. Data for water as displacing liquid and ternary solution as the confined liquid in both regimes is added for comparison (triangles).

are on a much larger scale (at least from 250 nm to 1 μm) due to the limitation of the spatial resolution.

The impacts of high ethanol content in the initial solution A are not studied in this work. We expect a high initial ethanol content to result in a composition path close to the axis from ethanol to water within the phase diagram. The reason is that the diffusive mixing may not generate enough concentration gradient for 1-octanol to form droplets. Therefore, no dynamic events due to phase separation may take place.

Using Water + Ethanol Binary Mixtures to Displace Solution A. Additional experiments were performed at high and low 1-octanol composition regime conditions using a displacing liquid containing 25% ethanol by mass in water. Figure 9A shows the approximate trajectory and associated tie

line from the dilution process with this displacing liquid for a regime 1 composition when water alone is used to displace it (see E1 in Table 2). The resulting water-rich phase formed by phase separation, in this case, has a composition corresponding to a regime 4 solution composition, while the composition of the 1-octanol-rich phase remains qualitatively similar.

Figure 9B shows an observed insoluble moving boundary and stranded 1-octanol-rich microdomains similar to the regime 1 behavior (Figure 3B) with fewer undulations. The smoother boundary displacement may be attributed to the reduction in the interfacial tensions and the pinning effect from the substrate with ethanol in the displacing liquid. Higher solubility of 1-octanol in ethanol solution may attribute to smaller microdomains.

Consistent results were also observed in Figure 9C, where solution A was 10% 1-octanol by mass, and the displacing liquid was 25% ethanol by mass solution (see E4 in Table 2). In this case, droplets formed behind the moving boundary and dissolved slowly due to the high solubility of 1-octanol in displacing liquid.

The boundary displacement as a function of time summarized in Figure 9D shows a time-invariant displacement rate for binary displacing liquid. Under conditions with water as the displacing liquid, the boundary displacement rate for regime 4 is 10 times greater, and for regime 1, the rate is 0.9 times lower. The faster displacement rate for regime 1 may be attributed to improvements in the solubility of 1-octanol in displacing liquid.

Displacing Water with Solution A. By displacing water with solution A (a 1-octanol-containing ternary mixture), we were able to consider impacts of reverse flow arising in large-scale porous media and to understand the impacts of relative wettability of the displacing liquid. Two cases, linked to experiments described in detail above, are illustrative.

Figure 10A shows the insoluble boundary arising when the confined liquid is water and the displacing liquid is solution A. The solution A composition corresponds to regime 1 (see R1 in Table 2) shown in Figure 3A. Droplets did not form within microdomains left behind by the boundary. Instead, small 1-octanol droplets were confined in the boundary zone, similar to regime 2 conditions in Figure 4. The boundary displacement rate was 9 times faster compared to that in normal regime 1 conditions.

Figure 10B shows the displacement boundary when solution A composition corresponds to regime 4 (see R4 in Table 2). In this case, 1-octanol-rich droplets and domains form at the boundary. The overall displacement rate of the boundary (Figure 10C) is time-invariant (77 μm/s) and 50 times faster than normal regime 4 conditions. This dramatic difference in displacement rate demonstrates that using displacing liquids with better wettability (lower interfacial tension) on the wall surface may provide an effective route to enhance fluid displacement rate in confinement. Such wettability manipulation is a common professional practice for enhanced oil recovery.[13]

CONCLUSIONS

We investigate the displacement process for phase separating ternary liquid mixtures in 2D confinement. The model mixtures contain 1-octanol (a model oil), water (a model poor solvent), and ethanol (a model good solvent), where water (the poor solvent) is the displacing fluid. One of the confining walls is hydrophobic, and the other is hydrophilic. Four composition-dependent displacement regimes are identified. While the details of the displacement mechanism corresponding to each regime differ, order of magnitude enhancements over single-phase diffusive displacement arise. The displacement rate was also shown to be further enhanced with the addition of ethanol (good solvent) to the displacing liquid, improving the wettability on the wall surface. Reverse flow cases where confined water is displaced with the ternary mixture further illustrate the importance of the impact of relative wettability of coexisting phases on boundary displacement. The findings in this work are readily generalized using phase diagrams to provide insights and guidelines for the design of solution formulations for confined liquid displacement. Such displacement processes are important in geological,

chemical, and biological processes in enhanced oil recovery, CO_2 sequestration, catalytic reactions, and drug delivery systems.

ASSOCIATED CONTENT

Ⓢ Supporting Information

The Supporting Information is available free of charge at https://pubs.acs.org/doi/10.1021/acs.energyfuels.1c00139.

> Videos of the boundary displacement in all four regimes (ZIP)
>
> Explanation to the thermodynamic calculations of excess free energy from phase separation; modified UNIFAC van der Waals parameters and interaction parameters used in calculations; solution flowrates used in symmetry calculations; compositions of 1-octanol-rich, water-rich, and bulk phases obtained from symmetry at different initial compositions; all chemical groups that were taken into account for UNIFAC excess enthalpy calculations; and time-based optical images of the early development of the three-zone configuration (PDF)

AUTHOR INFORMATION

Corresponding Author

Xuehua Zhang − *Department of Chemical and Materials Engineering, University of Alberta, Edmonton, Alberta T6G 1H9, Canada; Physics of Fluids Group, Max Planck Center Twente for Complex Fluid Dynamics, JM Burgers Center for Fluid Dynamics, Mesa+, Department of Science and Technology, University of Twente, Enschede 7522 NB, The Netherlands;* ◉ orcid.org/0000-0001-6093-5324; Email: xuehua.zhang@ualberta.ca

Authors

Gilmar F. Arends − *Department of Chemical and Materials Engineering, University of Alberta, Edmonton, Alberta T6G 1H9, Canada;* ◉ orcid.org/0000-0003-2066-7462

Jae Bem You − *Department of Chemical and Materials Engineering, University of Alberta, Edmonton, Alberta T6G 1H9, Canada;* ◉ orcid.org/0000-0003-0385-2295

John M. Shaw − *Department of Chemical and Materials Engineering, University of Alberta, Edmonton, Alberta T6G 1H9, Canada;* ◉ orcid.org/0000-0002-6176-4421

Complete contact information is available at:
https://pubs.acs.org/10.1021/acs.energyfuels.1c00139

Notes

The authors declare no competing financial interest.

REFERENCES

(1) Kortunov, P.; Vasenkov, S.; Kärger, J.; Fé Elía, M.; Perez, M.; Stöcker, M.; Papadopoulos, G. K.; Theodorou, D.; Drescher, B.; McElhiney, G.; Bernauer, B.; Krystl, V.; Kočiřík, M.; Zikánová, A.; Jirglová, H.; Berger, C.; Gläser, R.; Weitkamp, J.; Hansen, E. W. Diffusion in fluid catalytic cracking catalysts on various displacement scales and its role in catalytic performance. *Chem. Mater.* **2005**, *17*, 2466−2474.

(2) Tao, J.; Song, X.; Zhao, T.; Zhao, S.; Liu, H. Confinement effect on water transport in CNT membranes. *Chem. Eng. Sci.* **2018**, *192*, 1252−1259.

(3) Radhakrishnan, R.; Farokhirad, S.; Eckmann, D. M.; Ayyaswamy, P. S. Nanoparticle transport phenomena in confined flows. *Adv. Heat Transfer* **2019**, *51*, 55−129.

(4) Sanhai, W. R.; Sakamoto, J. H.; Canady, R.; Ferrari, M. Seven challenges for nanomedicine. *Nat. Nanotechnol.* **2008**, *3*, 242−244.

(5) Sparreboom, W.; van den Berg, A.; Eijkel, J. C. T. Principles and applications of nanofluidic transport. *Nat. Nanotechnol.* **2009**, *4*, 713−720.

(6) Wu, K.; Chen, Z.; Li, J.; Li, X.; Xu, J.; Dong, X. Wettability effect on nanoconfined water flow. *Proc. Natl. Acad. Sci. U.S.A.* **2017**, *114*, 3358−3363.

(7) Zhang, Y.; Yu, W.; Sepehrnoori, K.; Di, Y. Investigation of nanopore confinement on fluid flow in tight reservoirs. *J. Pet. Sci. Eng.* **2017**, *150*, 265−271.

(8) Druetta, P.; Picchioni, F. Surfactant flooding: The influence of the physical properties on the recovery efficiency. *Petroleum* **2020**, *6*, 149−162.

(9) Gao, J.; Xing, H.; Tian, Z.; Pearce, J. K.; Sedek, M.; Golding, S. D.; Rudolph, V. Reactive transport in porous media for CO2 sequestration: Pore scale modeling using the lattice Boltzmann method. *Comput. Geosci.* **2017**, *98*, 9−20.

(10) Feng, D.; Wu, K.; Wang, X.; Li, J.; Li, X. Modeling the confined fluid flow in micro-nanoporous media under geological temperature and pressure. *Int. J. Heat Mass Transfer* **2019**, *145*, 118758.

(11) Tartakovsky, D. M.; Dentz, M. Diffusion in Porous Media: Phenomena and Mechanisms. *Transp. Porous Media* **2019**, *130*, 105−127.

(12) Fredriksen, S. B.; Rognmo, A. U.; Fernø, M. A. Pore-scale mechanisms during low salinity waterflooding: Oil mobilization by diffusion and osmosis. *J. Pet. Sci. Eng.* **2018**, *163*, 650−660.

(13) Aziz, R.; Niasar, V.; Erfani, H.; Martínez-Ferrer, P. J. Impact of pore morphology on two-phase flow dynamics under wettability alteration. *Fuel* **2020**, *268*, 117315.

(14) Ho, T. A.; Wang, Y. Enhancement of oil flow in shale nanopores by manipulating friction and viscosity. *Phys. Chem. Chem. Phys.* **2019**, *21*, 12777−12786.

(15) Guillen, V. R.; Carvalho, M. S.; Alvarado, V. Pore scale and macroscopic displacement mechanisms in emulsion flooding. *Transp. Porous Media* **2012**, *94*, 197−206.

(16) Xu, W.; Ok, J. T.; Xiao, F.; Neeves, K. B.; Yin, X. Effect of pore geometry and interfacial tension on water-oil displacement efficiency in oil-wet microfluidic porous media analogs. *Phys. Fluids* **2014**, *26*, 093102.

(17) Zhou, Y.; Yin, D.; Chen, W.; Liu, B.; Zhang, X. A comprehensive review of emulsion and its field application for enhanced oil recovery. *Energy Sci. Eng.* **2019**, *7*, 1046−1058.

(18) Mandal, A.; Samanta, A.; Bera, A.; Ojha, K. Characterization of oil−water emulsion and its use in enhanced oil recovery. *Ind. Eng. Chem. Res.* **2010**, *49*, 12756−12761.

(19) Lohse, D.; Zhang, X. Physicochemical hydrodynamics of droplets out of equilibrium. *Nat. Rev. Phys.* **2020**, *2*, 426−443.

(20) Shi, N.; Nery-Azevedo, R.; Abdel-Fattah, A. I.; Squires, T. Diffusiophoretic focusing of suspended colloids. *Phys. Rev. Lett.* **2016**, *117*, 258001.

(21) Nery-Azevedo, R.; Banerjee, A.; Squires, T. M. Diffusiophoresis in ionic surfactant gradients. *Langmuir* **2017**, *33*, 9694−9702.

(22) Banerjee, A.; Williams, I.; Azevedo, R. N.; Helgeson, M. E.; Squires, T. M. Soluto-inertial phenomena: Designing long-range, long-lasting, surface-specific interactions in suspensions. *Proc. Natl. Acad. Sci. U.S.A.* **2016**, *113*, 8612−8617.

(23) Kar, A.; Chiang, T.-Y.; Ortiz Rivera, I.; Sen, A.; Velegol, D. Enhanced Transport into and out of Dead-End Pores. *ACS Nano* **2015**, *9*, 746−753.

(24) Shin, S.; Um, E.; Sabass, B.; Ault, J. T.; Rahimi, M.; Warren, P. B.; Stone, H. A. Size-dependent control of colloid transport via solute gradients in dead-end channels. *Proc. Natl. Acad. Sci. U.S.A.* **2016**, *113*, 257−261.

(25) Ault, J. T.; Shin, S.; Stone, H. A. Diffusiophoresis in narrow channel flows. *J. Fluid Mech.* **2018**, *854*, 420−448.

(26) Vitale, S. A.; Katz, J. L. Liquid Droplet Dispersions Formed by Homogeneous Liquid-Liquid Nucleation: "The Ouzo Effect". *Langmuir* **2003**, *19*, 4105−4110.

(27) Lu, Z.; Schaarsberg, M. H. K.; Zhu, X.; Yeo, L. Y.; Lohse, D.; Zhang, X. Universal Nanodroplet Branches from Confining the Ouzo Effect. *Proc. Natl. Acad. Sci. U.S.A.* **2017**, *114*, 10332−10337.

(28) Zemb, T. N.; Klossek, M.; Lopian, T.; Marcus, J.; Schöettl, S.; Horinek, D.; Prevost, S. F.; Touraud, D.; Diat, O.; Marčelja, S.; Kunz, W. How to Explain Microemulsions Formed by Solvent Mixtures without Conventional Surfactants. *Proc. Natl. Acad. Sci. U.S.A.* **2016**, *113*, 4260−4265.

(29) Zhang, X. H.; Ducker, W. Interfacial oil droplets. *Langmuir* **2008**, *24*, 110−115.

(30) Lopian, T.; Schöttl, S.; Prévost, S.; Pellet-Rostaing, S.; Horinek, D.; Kunz, W.; Zemb, T. Morphologies Observed in Ultraflexible Microemulsions with and without the Presence of a Strong Acid. *ACS Cent. Sci.* **2016**, *2*, 467−475.

(31) Pratt, K. C.; Wakeham, W. A. The Mutual Diffusion Coefficient of Ethanol−Water Mixtures: Determination by a Rapid, New Method. *Proc. R. Soc. London, Ser. A* **1974**, *336*, 393−406.

(32) Kinoshita, K.; Parra, E.; Needham, D. New sensitive micro-measurements of dynamic surface tension and diffusion coefficients: Validated and tested for the adsorption of 1-Octanol at a microscopic air-water interface and its dissolution into water. *J. Colloid Interface Sci.* **2017**, *488*, 166−179.

(33) Su, J. T.; Duncan, P. B.; Momaya, A.; Jutila, A.; Needham, D. The effect of hydrogen bonding on the diffusion of water in n-alkanes and n-alcohols measured with a novel single microdroplet method. *J. Chem. Phys.* **2010**, *132*, 044506.

(34) Li, M.; Bao, L.; Yu, H.; Zhang, X. Formation of Multi-component Surface Nanodroplets by Solvent Exchange. *J. Phys. Chem. C* **2018**, *122*, 8647−8654.

(35) Lu, Z.; Xu, H.; Zeng, H.; Zhang, X. Solvent Effects on the Formation of Surface Nanodroplets by Solvent Exchange. *Langmuir* **2015**, *31*, 12120−12125.

(36) Diat, O.; Klossek, M. L.; Touraud, D.; Deme, B.; Grillo, I.; Kunz, W.; Zemb, T. Octanol-rich and water-rich domains in dynamic equilibrium in the pre-ouzo region of ternary systems containing a hydrotrope. *J. Appl. Crystallogr.* **2013**, *46*, 1665−1669.

(37) Schöttl, S.; Marcus, J.; Diat, O.; Touraud, D.; Kunz, W.; Zemb, T.; Horinek, D. Emergence of surfactant-free micelles from ternary solutions. *Chem. Sci.* **2014**, *5*, 2949−2954.

(38) Prevost, S.; Lopian, T.; Pleines, M.; Diat, O.; Zemb, T. Small-angle scattering and morphologies of ultra-flexible microemulsions. *J. Appl. Crystallogr.* **2016**, *49*, 2063−2072.